Supporting Information

Dynamic structural evolution of soft colloidal monolayers under uniaxial compression

Below we describe details on the experimental methodology for LT-SALS. A full compression isotherm of CS microgels (the main system used in the manuscript) was constructed from two separate experiments in **Fig S1** with additional experimental details in **Table S1**. **Fig S2** compares slow and fast compression of the CS microgels, highlighting the anisotropy and hysteresis observed in the fast compression, while **Fig 3** describes reciprocal lattice vectors, angle between them, and rotation angles are measured. Below are the equations used to calculate interparticle distances from diffraction patterns. Reproducibility of the observed 30° lattice reorientation is also confirmed through three consecutive compression-expansion cycles performed on a different system: CS2 microgels (**Fig S4**, with silica core sized 437 nm in diameter and overall hydrodynamic diameter of 1003 nm with shell crosslinker density of 2.5 mol.%). Complementary ex situ characterization via optical microscopy of monolayers transferred onto hydrophobically modified glass substrates (using both Langmuir-Blodgett and Langmuir-Schäfer deposition techniques) enables stretch of the interfacial structures (**Fig S5** and **S6**).

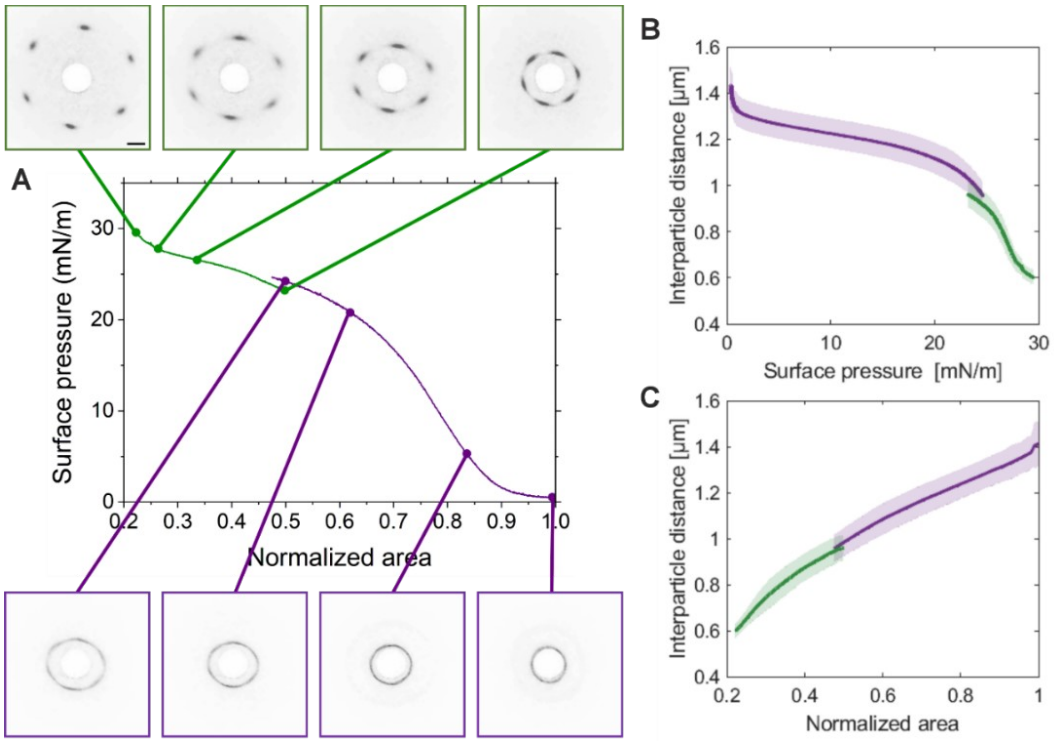

Figure S1. **A**) Compression isotherm of CS monolayer recorded by LT-SALS. Due to limitations in the trough size, the compression isotherm was constructed from two separate compression experiments. The first compression (violet) began with a lower number density, while the second (green) started at three times the initial concentration. The two isotherms were connected using the same average nearest-neighbour centre-to-centre distance (interparticle distance) calculated from the diffraction patterns (insets). The trough area at the corresponding time was normalized to 0.5 to create a continuous isotherm. The scale bar corresponds to 10 mm. **B**) Interparticle distance versus surface pressure plot for the same set of data, **C**) Interparticle distance versus normalized trough area. The shaded bands are uncertainty propagated from the Gaussian fit full width at half maximum.

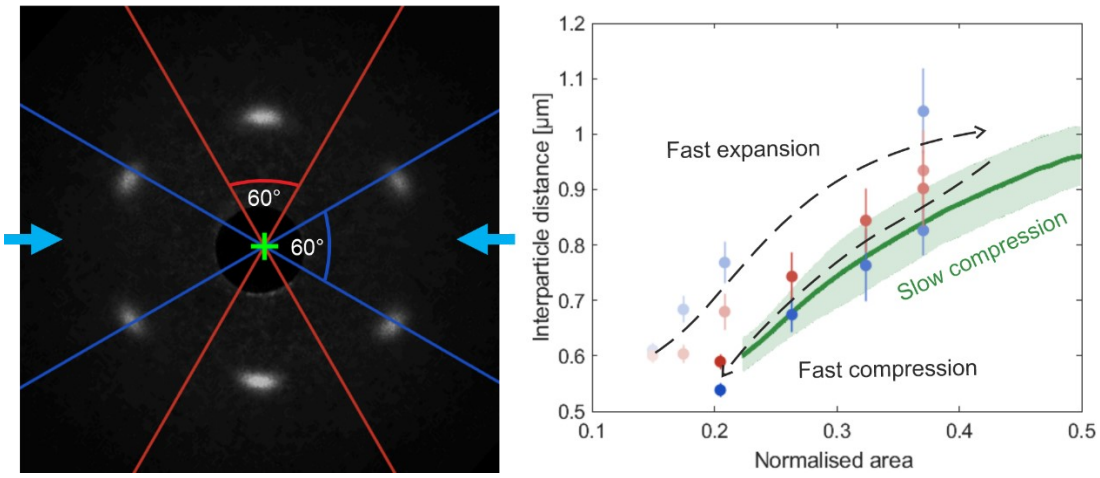

Figure S2. Structural response of the CS monolayer to slow (1 mm/min near equilibrium, Figure 2) versus fast (27 mm/min out-of-equilibrium dynamic, Figure 4) compression. (Left) Representative angular-sectors (trough length direction, i.e., perpendicular to the compression direction: blue, width direction, i.e., parallel to the compression direction: red) definition overlaid on a SALS diffraction pattern taken during the rapid expansion-compression cycle. (Right) Interparticle distance as a function of normalized trough area. The green band shows the slow equilibrium compression from Figure 2. the curve terminates at normalized trough area ≈ 0.22 where the experiment was stopped followed by relaxation for 30 min, and then further compressed back to a measured surface pressure of 30 mN/m. Colored markers show eight selected frames of a subsequent fast opening-and-closing cycle performed on the same monolayer from Figure 4, with interparticle distance calculated from the trough length direction (blue) and width direction (red). The different shadings of the symbols encode the temporal order of the cycle. The fast-expansion branch lies above the slow-compression curve, defining a hysteresis loop (dashed path, guide to the eye) with a pronounced anisotropy of the diffraction pattern. Notably, the relative ordering of the two sector directions swaps between the expansion and compression legs: during fast expansion the trough-length (blue) direction exhibits the larger interparticle distance, whereas

during fast re-compression the trough-width (red) direction becomes dominant. This inversion indicates that the rapid deformation drives the monolayer through distinct anisotropic states that equilibrium compression does not access.

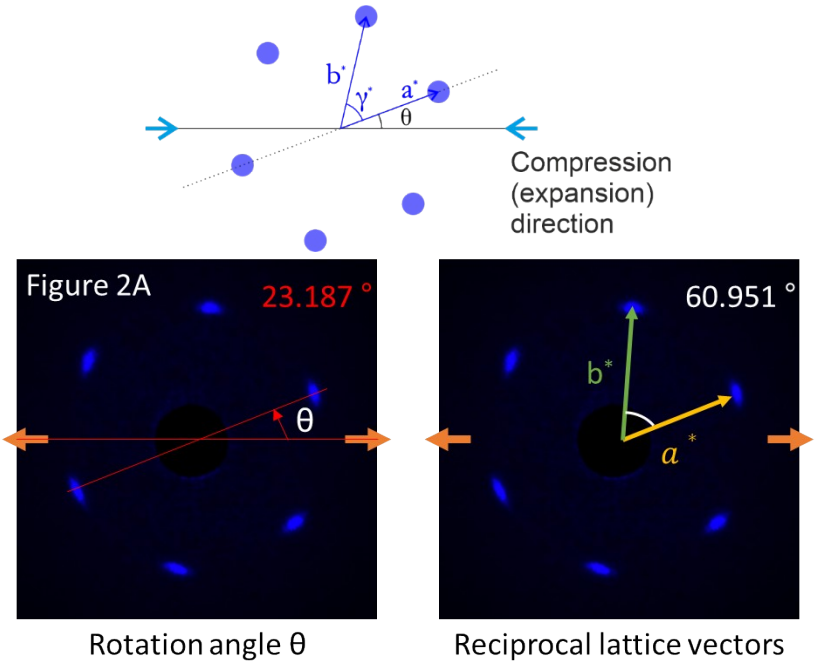

Figure S3. Reciprocal lattice vectors a^* and b^* and the angle between them, γ^*, are used to calculate the real space lattice vectors a and b and their corresponding angle, γ. The rotation angle, θ, is determined to align the calculated real space lattice with the observed diffraction patterns. Below the diffraction pattern of Figure 2A is shown as an example for measuring the vectors and rotation angle.

Table S1. LT-SALS. Additional experimental details for **Figures 2**, **4** and **6** of the main manuscript.

Figure 2.		**A**	**B**	**C**	**D**
LT	Barrier position [mm]	0.1	55.3	75.1	90.1

	Area %	100	65	53	43
	Surface pressure [mN/m]	23.2	26.6	27.6	29.6
SALS	$d_{c\text{-}c}$ [µm]	0.96	0.78	0.69	0.60
	$d_{c\text{-}c}$, std [µm]	0.08	0.08	0.05	0.04
	Aspect ratio	1.06	1.16	1.16	1.15

Figure 4.		**A**	**B**	**C**	**D**	**E**	**F**	**G**	**H**
LT	Barrier position [mm]	110.0	101.9	91.0	38.4	38.4	53.6	73.2	92.1
	Area %	31	36	43	76	76	66	54	42
SALS	$d_{c\text{-}c}$ [µm]	0.61	0.68	0.74	1.01	0.89	0.84	0.72	0.56
	$d_{c\text{-}c}$, std [µm]	0.02	0.03	0.07	0.10	0.09	0.07	0.07	0.02
	Aspect ratio	1.02	1.34	1.27	1.17	1.18	1.23	1.22	1.31

The interparticle distance measured by LT-SALS, $d_{c\text{-}c}$, was calculated as follows:

$$q = \frac{4\pi n}{\lambda} \sin\left(\frac{\operatorname{atan}\left(\frac{x}{d_{S-D}}\right)}{2}\right)$$

where q is the magnitude of the scattering vector, n the refractive index, λ the wavelength of the laser (405 nm), x the radially averaged peak position, $d_{S\text{-}D}$ the sample-to-detector distance. The lattice spacing $d_{hk} = \frac{2\pi}{q}$ and for hexagonal arrays, the interparticle distance $d_{c-c} = \frac{2}{\sqrt{3}} d_{hk}$.

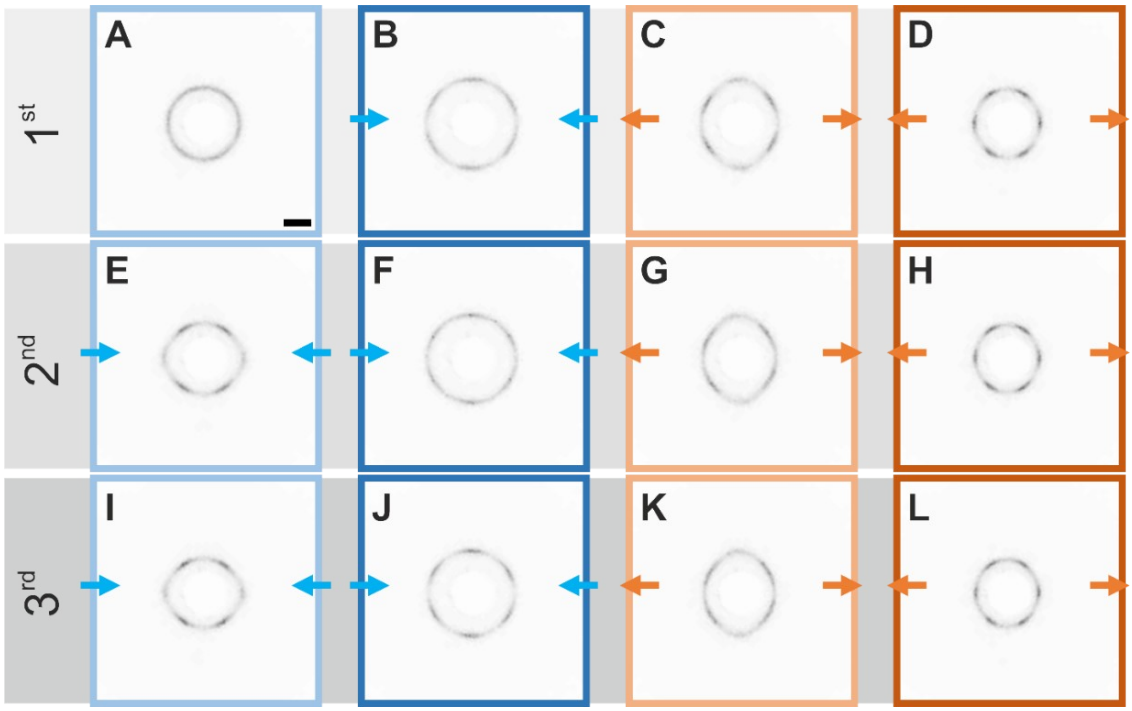

Figure S4. Three consecutive expansion-compression cycles of the CS2 microgel monolayer, recorded via LT-SALS at a compression/expansion speed of 9 mm/min. The blue arrows indicate compression, while the orange arrows indicate expansion. **A-D**) correspond to the first, **E-H**) to the second, and **I-L**) to the third cycle. The scale bar corresponds to 10 mm.

Table S2. LT-SALS additional experimental details for Figure S3.

Figure S3.		**A**	**B**	**C**	**D**	**E**
LT	Barrier position [mm]	0	50	34.5	0	22.1
	Area %	100	69	78	100	86
	Surface pressure	27.4	28.6	27.8	26.8	27.8
SALS	$d_{c\text{-}c}$ [µm]	1.10	0.91	1.01	1.16	1.09
	$d_{c\text{-}c}$, std [µm]	0.06	0.04	0.06	0.07	0.07
	Aspect ratio	1.00	1.04	1.17	1.09	1.11

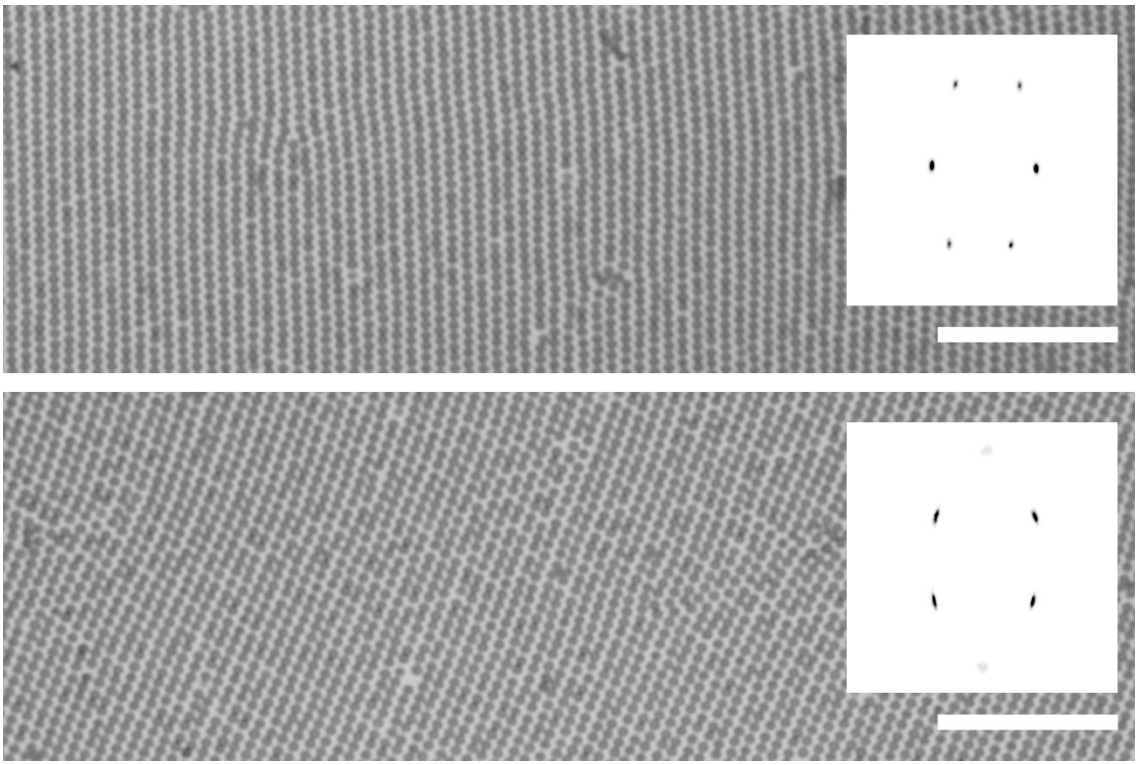

Figure S5. Light microscopy of CS3 (silica core sized 340 nm in diameter and overall hydrodynamic diameter of 1020 nm with shell crosslinker density of 5.2 mol.%) monolayer transferred on a surface-modified glass substrate with 1H,1H,2H,2H-perfluorodecyltriethoxysilane (below simply referred to as hydrophobic) via Langmuir–Blodgett deposition (Microtrough G2, Kibron Inc., barrier speed at 40 mm/min, dipper speed 10 mm/min) at a constant surface pressure of approx. 30 mM/m at two different and representative locations. The inserts are SALS diffraction patterns of the monolayer at the corresponding locations. The scale bar corresponds to 10 μm.

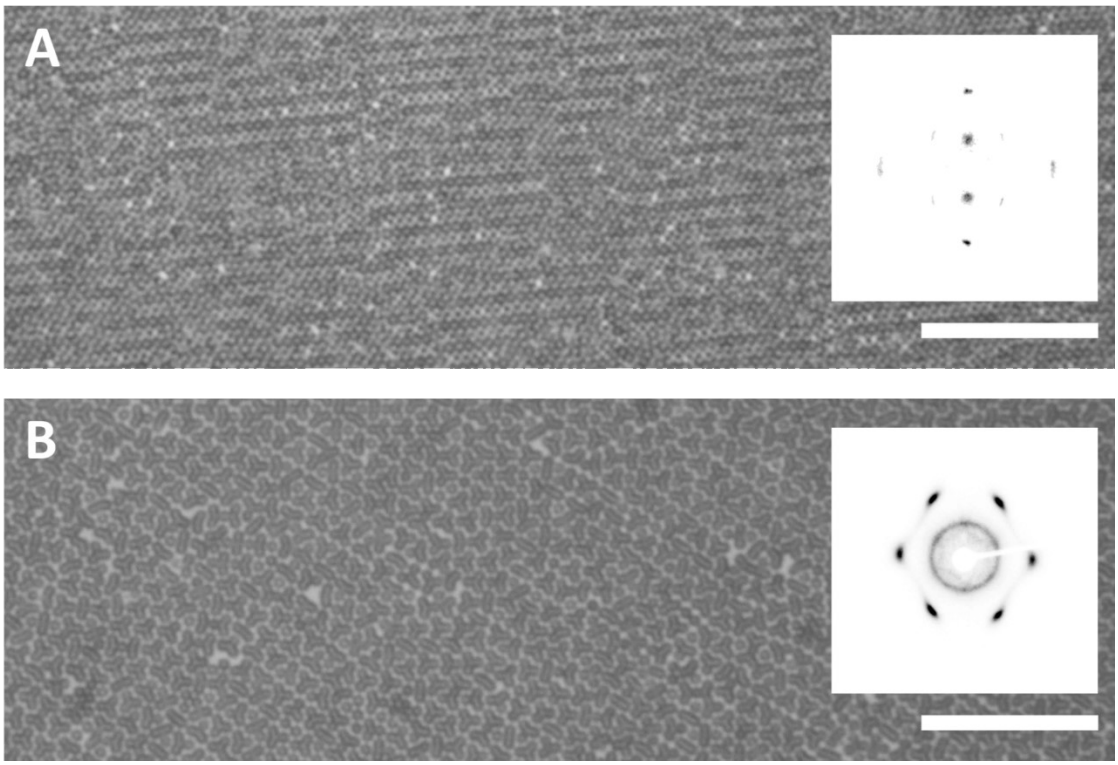

Figure S6. A) Light microscopy of a monolayer made by double deposition: 1) CS3 monolayer transfer at 30 mN/m on a hydrophobic glass substrate via reverse Langmuir-Blodgett deposition as above, 2) followed by thorough cleaning of the interface with an aspirator while the substrate was fully immersed, 3) interface-mediated assembly of the CS microgels to 30 mN/m and then the second deposition was done at a constant surface pressure of approx. 30 mM/m on the top of CS3 monolayer. **B)** CS3 monolayer transfer at 30 mN/m on a hydrophobic glass substrate via Langmuir-Schäfer deposition. The inserts are SALS diffraction patterns of the monolayer at the locations. The scale bar corresponds to 10 μm.